Disorder-induced broadening of excitonic resonances in transition metal dichalcogenides

Magdulin Dwedari,[1,*] Samuel Brem,[2] Maja Feierabend,[2] and Ermin Malic[2]
[1]*Department of Physics, University Duisburg-Essen, 47048 Duisburg, Germany*
[2]*Department of Physics, Chalmers University of Technology, 412 96 Gothenburg, Sweden*

(Received 22 March 2019; revised manuscript received 28 May 2019; published 17 July 2019)

The presence of impurities and disorder has an important impact on the optical response of monolayer transition metal dichalcogenides (TMDs). Here, we investigate elastic exciton-impurity scattering and its influence on the linewidth of excitonic resonances in different TMD materials. We derive an analytic expression for the linewidth broadening within the density matrix formalism. We find that the exciton linewidth increases for states up to the 3*s* exciton due to the scattering with impurities. For higher states, the impurity contribution decreases, reflecting the reduced scattering cross section. Furthermore, we reveal that the scattering efficiency is the largest for transitions between *s* and *p* exciton states. Finally, different TMDs show generally a similar behavior. The quantitatively smaller broadening in tungsten-based TMDs can be ascribed to their smaller effective masses resulting in a less efficient scattering.

DOI: 10.1103/PhysRevMaterials.3.074004

I. INTRODUCTION

Atomically thin monolayers of transition metal dichalcogenides show an exceptional optical response due to high exciton binding energies of a few hundreds of meV, resulting from the reduced Coulomb screening in the low-dimensional configuration. Many studies have investigated the linewidths of excitonic resonances revealing the underlying many-particle scattering processes, such as exciton-exciton, radiative recombination, and exciton-phonon scattering [1–4], whereas disorder scattering has been rather disregarded. Despite the improvement of the fabrication techniques of TMD monolayers, it is impossible to entirely eliminate imperfections [5]. Disorder is present in every sample at any temperature [6–8], making it a crucial aspect to exciton dynamics. In particular, inhomogeneities in the substrate, e.g., spatial fluctuations of the dielectric constant, lead to statistical fluctuations of resonance energies throughout the sample giving rise to an inhomogeneous broadening. In addition, lattice defects such as vacancies or impurities, can contribute to a homogeneous broadening resulting from elastic scattering of excitons at the electrostatic potential induced by the defects. The broadening of the exciton ground state is usually dominated by exciton-phonon scattering, radiative recombination [9,10], and inhomogeneous broadening mechanisms resulting from the above-mentioned fluctuations of the resonance energy. Since elastic scattering with impurities requires a resonant scattering channel, these processes are strongly suppressed in the ground state. However, for higher excitonic states the impact of impurity-assisted scattering becomes important since we find here a larger number of possible resonant scattering channels, cf. Fig. 1. While in previous studies we have focused on the intrinsic broadening mechanism in TMD monolayers, we examine here the impact of extrinsic defects in the linewidth of excitons. In particular, we theoretically investigate the impact of the elastic exciton-impurity scattering on the absorption spectrum of different TMD monolayer materials. The goal is to obtain an analytic expression for the impurity-induced homogeneous broadening of excitonic linewidths and to investigate the dependence on the exciton quantum number *n* as well as the differences for the four most studied semiconducting TMD materials (WS_2, WSe_2, MoS_2, $MoSe_2$).

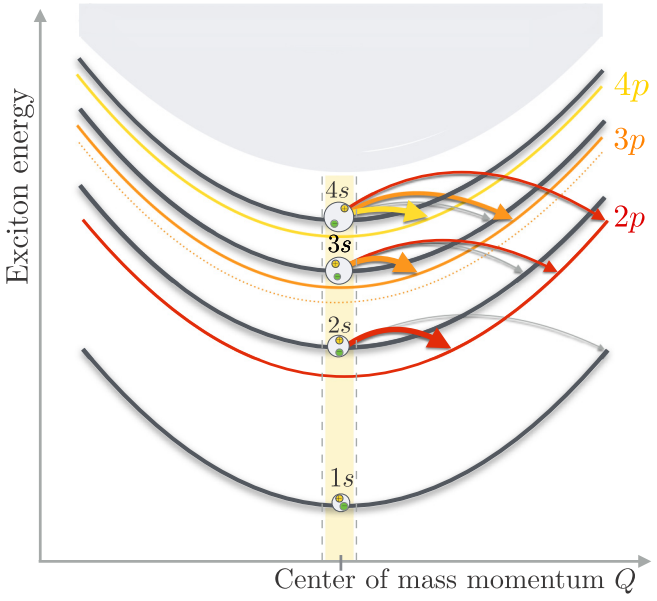

FIG. 1. Schematic illustration of elastic impurity scattering channels for the first four *s* excitonic states. An optically excited exciton with zero center of mass momentum (yellow area) can scatter elastically into the possible resonant states by a momentum transfer introduced by impurities. The 1*s* state has no resonant scattering partners. The thickness of the arrows indicates the strengths of the scattering efficiency.

*magdulin.dwedari@uni-due.de

II. THEORETICAL APPROACH

The strong Coulomb interaction between electrons and holes results in a series of optical (excitonic) resonances and a Rydberg-like series similar to the hydrogen atom [11]. Excitonic resonances have a characteristic width reflecting the dephasing time of the microscopic polarization corresponding to the lifetime of coherent excitons [10]. We distinguish between inhomogeneous and homogeneous broadening processes. While the first result from statistical fluctuations of resonance energies throughout the investigated sample, the latter are given by exciton-phonon scattering, radiative recombination, and exciton-exciton scattering that becomes important at high excitations. In addition, elastic exciton-impurity scattering can significantly contribute to the homogeneous broadening. This scattering mechanism is in the focus of this work.

We start our study by investigating the absorption coefficient $\alpha(\omega)$. An optical perturbation caused by an external vector potential $A(\omega)$ induces a response according to the optical susceptibility $\chi(\omega)$ of the material resulting in [12–14]

$$\alpha(\omega) \propto \omega \Im[\chi(\omega)] \propto \frac{1}{\omega} \Im \sum_{i,j} M_{ij} p_{ij}(\omega), \tag{1}$$

where M_{ij} is the optical matrix element with the compound index $i = \{\lambda, \mathbf{k}\}$ for the band λ and the momentum $\mathbf{k}$. The quantity $p_{ij} = p^{\lambda\ \lambda'}_{\mathbf{k}\ \mathbf{k}'} = \langle a^\dagger_{\lambda\mathbf{k}} a_{\lambda'\mathbf{k}'} \rangle$ is the microscopic polarization, which is given by the expectation value of the transition from the electronic state $|\lambda'\mathbf{k}'\rangle$ to $|\lambda\mathbf{k}\rangle$. To obtain the time dependence of this quantity, we exploit the Heisenberg equation [12,15–17] $\dot{p}^{\lambda\ \lambda'}_{\mathbf{k}\ \mathbf{k}'} = \frac{i}{\hbar}\langle [H, p^{\lambda\ \lambda'}_{\mathbf{k}\ \mathbf{k}'}] \rangle$ and consider the many-particle Hamilton operator [13,18] $H = H_{0,e} + H_{e,e} + H_{e-f} + H_\mathrm{d}$. The latter includes the noninteraction electron ($H_{0,e}$), the electron-electron ($H_{e,e}$) and the electron-light interaction H_{e-f} as well as the exciton-disorder coupling [19,20]

$$H_\mathrm{d} = \sum_{\lambda\lambda',\mathbf{k}\mathbf{k}'} \mathcal{D}^{\lambda\lambda'}_{\mathbf{k}\mathbf{k}'} a^\dagger_{\lambda\mathbf{k}} a_{\lambda'\mathbf{k}'}. \tag{2}$$

The operators $a^\dagger_{\lambda\mathbf{k}}$ and $a_{\lambda'\mathbf{k}'}$ are the electron creation and annihilation operators, respectively. The appearing disorder matrix element $\mathcal{D}^{\lambda\lambda'}_{\mathbf{k}\mathbf{k}'}$ indicates the strength of the transition due to scattering on impurities and is given by

$$\mathcal{D}^{\lambda\lambda'}_{\mathbf{k}\mathbf{k}'} = \langle \lambda\mathbf{k}| U(\mathbf{r}) |\lambda'\mathbf{k}'\rangle = \frac{1}{V} \sum_{\mathbf{q}} U_{\mathbf{q}} \langle \lambda\mathbf{k}| e^{i\mathbf{q}\cdot\mathbf{r}} |\lambda'\mathbf{k}'\rangle, \tag{3}$$

where $U(\mathbf{r})$ is the disorder potential [19,20] and V the volume. To keep the study general, we do not assume a specific $U(\mathbf{r})$, but only require that the potential possesses the properties of white noise, where a disorder average results in $\overline{U(\mathbf{r})} = 0$, $\overline{U(\mathbf{r})U(\mathbf{r}')} = D_0^2 V \delta(\mathbf{r} - \mathbf{r}')$ with $D_0^2 = \rho_\mathrm{d} u^2$, where u is the strength of the disorder potential and ρ_d the density of impurities, which we consider to be low.

In vicinity of minima and maxima of the electronic band structure, we apply the effective mass model, so that wave functions are well approximated by plane waves. For small momentum transfers this yields $\mathcal{D}^{\lambda\ \lambda'}_{\mathbf{k}\ \mathbf{k}'} = \frac{1}{V^2}\delta_{\lambda,\lambda'} \sum_{\mathbf{q}} U_{\mathbf{q}} \delta_{\mathbf{k}',\mathbf{k}+\mathbf{q}}$ where $\delta_{\lambda,\lambda'}$ results from the rotating wave approximation, only allowing intraband transitions. Now, the disorder Hamiltonian can be simplified to

$$H_\mathrm{d} = \sum_{\lambda\mathbf{k}\mathbf{q}} \mathcal{D}_{\mathbf{q}} a^\dagger_{\lambda\mathbf{k}} a_{\lambda,\mathbf{k}+\mathbf{q}}.$$

Applying the Heisenberg equation, we obtain the disorder contribution of the semiconductor Bloch equation

$$\dot{p}^{\lambda\lambda'}_{\mathbf{k}\mathbf{k}'}\big|_{H_\mathrm{d}} = \frac{i}{\hbar} \sum_{\mathbf{q}} \mathcal{D}_{\mathbf{q}} \left(p^{\lambda\lambda'}_{\mathbf{k}-\mathbf{q}\mathbf{k}'} - p^{\lambda\lambda'}_{\mathbf{k}\mathbf{k}'+\mathbf{q}} \right). \tag{4}$$

To account for the strong Coulomb interaction in TMDs, we transform the results into an excitonic basis [21]. First, we define center-of-mass $\mathbf{Q} = \mathbf{k} - \mathbf{k}'$ and relative momenta $\mathbf{q} = \beta\mathbf{k} + \alpha\mathbf{k}'$ with $\alpha = m_v/(m_v + m_c)$ and $\beta = m_c/(m_v + m_c)$ with the effective conduction and valence band masses m_c, m_v. The microscopic polarization then reads $p_{\mathbf{q},\mathbf{Q}}(t) = \sum_\nu \Phi^\nu_{\mathbf{q}} p^\nu_{\mathbf{Q}}(t)$, where the sum ν runs over all excitonic states. The excitonic wave functions $\Phi^\nu_{\mathbf{q}}$ as well as the excitonic energies E^ν are obtained by solving the Wannier equation [12,22,23], where we have considered TMD on silicon dioxide with a dielectric constant of $\epsilon_{\mathrm{SiO}_2} = 3.9$. Then, the semiconductor Bloch equation [12] for the excitonic polarization $p^\mu_{\mathbf{Q}}(t)$ reads

$$\dot{p}^\mu_{\mathbf{Q}}(t) = \frac{i}{\hbar}\left(E^\mu + \frac{\hbar^2\mathbf{Q}^2}{2M} \right) p^\mu_{\mathbf{Q}}(t) + \Omega^\mu(t)\delta_{\mathbf{Q},0} + \sum_{\nu,\mathbf{Q}'} D^{\mu\nu}_{\mathbf{Q}'}\ p^\nu_{\mathbf{Q}-\mathbf{Q}'}(t). \tag{5}$$

The first term describes the dispersion relation of excitons with the binding energy E^μ and the kinetic energy of its center-of-mass motion, where $M = m_c + m_v$ is the total mass. The Rabi-frequency $\Omega^\mu(t) = \frac{ie_0\hbar}{m} \sum_{\mathbf{q}} \Phi^{\mu *}_{\mathbf{q}} \mathbf{M}^{cv}_{\mathbf{q}} \cdot \mathbf{A}(t)$ expresses the excitation of the polarization due to an external vector potential $\mathbf{A}(t)$ with the elementary charge e_0 and the free electron mass m. The appearing Kronecker $\delta_{\mathbf{Q},0}$ accounts for the negligibly small photon momentum requiring $\mathbf{k}' = \mathbf{k}$ and $\mathbf{Q} = 0$. Finally, the disorder term couples the polarizations with different center-of-mass momenta, where $\mathbf{Q}'$ describes the momentum transfer due to exciton-impurity scattering. In the excitonic basis, the disorder scattering matrix reads

$$D^{\mu\nu}_{\mathbf{Q}'} = \frac{i}{\hbar V^2} U_{\mathbf{Q}'} \sum_{\mathbf{q}} \left[\Phi^{\mu *}_{\mathbf{q}} \left(\Phi^\nu_{\mathbf{q}-\beta\mathbf{Q}'} - \Phi^\nu_{\mathbf{q}+\alpha\mathbf{Q}'} \right) \right]. \tag{6}$$

This illustrates that the impurity-induced excitonic transition $\mu \to \nu$ strongly depends on the wave function overlap of the involved states. Note that the disorder scattering matrix does not depend on the excitonic momentum $\mathbf{Q}$, but only on the momentum transfer $\mathbf{Q}'$ due to impurity scattering. Additionally, we only consider small momentum transfer not sufficient to scatter excitons into dark states. This is a reasonable assumption as it translates to a low impurity density in real space, which is desirable in fabrication of clean samples.

A typical measurement of the absorption spectrum considers the sample as a whole and the revealed quantities are in fact an average over the sample. Here, we perform an ensemble average, i.e., Eq. (5) is solved for different configurations of $U(\mathbf{r})$ (different samples) and an average over all solutions is performed. This is equivalent to solving

the equation for different areas of the sample and performing the spatial average. Since the zeroth order of the correlation expansion $\overline{D_{\mathbf{Q}'}\, p_{\mathbf{Q}-\mathbf{Q}'}} = \overline{D_{\mathbf{Q}'}} \cdot \overline{p_{\mathbf{Q}-\mathbf{Q}'}} + \overline{D_{\mathbf{Q}'}\, p_{\mathbf{Q}-\mathbf{Q}'}}^{c}$ vanishes due to the white noise property of the impurity potential, we calculate the temporal evolution of the correlated part [24]

$$\frac{d}{dt}\overline{D^{\mu\nu}_{\mathbf{Q}'} p^{\nu}_{\mathbf{Q}-\mathbf{Q}'}}^{c}(t) \approx \frac{i}{\hbar}\left(E^{\nu} + \frac{\hbar^2(\mathbf{Q}-\mathbf{Q}')^2}{2M}\right)\overline{D^{\mu\nu}_{\mathbf{Q}'} p^{\nu}_{\mathbf{Q}-\mathbf{Q}'}}^{c}(t) + \sum_{\lambda\mathbf{K}} \overline{D^{\mu\nu}_{\mathbf{Q}'} D^{\nu\lambda}_{\mathbf{K}}}\; \overline{p^{\lambda}_{\mathbf{Q}-\mathbf{Q}'-\mathbf{K}}(t)}. \tag{7}$$

The last term is an approximation, since the correlated part of the average is neglected (second-order Born approximation) to break the hierarchy $\frac{d}{dt}\overline{D_1 \ldots D_n p} \propto \overline{D_1 \ldots D_{n+1} p}$. To account for this neglected correlation, a damping term is phenomenologically added to the equation. Fourier transforming this equation leads to

$$\sum_{\mathbf{Q}'} \overline{D^{\mu\nu}_{\mathbf{Q}'} p^{\nu}_{\mathbf{Q}-\mathbf{Q}'}(\omega)}^{c} \approx \sum_{\lambda\mathbf{Q}',\mathbf{K}} \frac{\overline{D^{\mu\nu}_{\mathbf{Q}'} D^{\nu\lambda}_{\mathbf{K}}}\; \overline{p^{\lambda}_{\mathbf{Q}-\mathbf{Q}'-\mathbf{K}}(\omega)}}{\frac{i}{\hbar}\left[\Delta E^{\nu}_{\mathbf{Q}-\mathbf{Q}'}(\omega) - i\delta^{\nu}_{\mathbf{Q}}(\omega)\right]},$$

where we have introduced the abbreviation $\Delta E^{\nu}_{\mathbf{Q}-\mathbf{Q}'}(\omega) = \hbar\omega - E^{\nu} - \frac{\hbar^2(\mathbf{Q}-\mathbf{Q}')^2}{2M}$ and the damping rate $\delta^{\nu}_{\mathbf{Q}}(\omega)$. Inserting this result back into the averaged, Fourier transformed Bloch equation and only considering the diagonal contribution yields

$$\overline{p^{\mu}_{\mathbf{Q}=0}(\omega)} = \frac{-i\hbar\Omega^{\mu}(\omega)}{\hbar\omega - E^{\mu} + \left(\hbar^2 \sum_{\nu,\mathbf{Q}'} \frac{\overline{|D^{\mu\nu}_{\mathbf{Q}'}|^2}}{\left[\Delta E^{\nu}_{\mathbf{Q}'}(\omega) - i\delta^{\nu}\right]}\right)}. \tag{8}$$

Now, we can identify the broadening of the exciton state μ as $i\gamma^{\mu}(\omega) = \hbar^2 \sum_{\nu,\mathbf{Q}'} \frac{\overline{|D^{\mu\nu}_{\mathbf{Q}'}|^2}}{\Delta E^{\nu}_{\mathbf{Q}'}(\omega) - i\delta^{\nu}}$. In the following we only consider perfectly elastic scattering processes (Markov approximation) with $\delta \to 0$ and neglect energy renormalization terms given by the real part. Therewith, we obtain an analytic expression for the broadening of excitonic resonances caused by elastic disorder scattering

$$\gamma^{\mu} = \pi D_0^2 \sum_{\nu\mathbf{Q}} \left|\mathcal{F}^{\mu\nu}_{\mathbf{Q}}\right|^2 \delta\left(E^{\nu} + \frac{\hbar^2\mathbf{Q}^2}{2M} - E^{\mu}\right) \tag{9}$$

with the dimensionless form factor $\mathcal{F}^{\mu\nu}_{\mathbf{Q}} = 1/V \sum_{\mathbf{q}} \Phi^{\mu *}_{\mathbf{q}} (\Phi^{\nu}_{\mathbf{q}-\beta\mathbf{Q}} - \Phi^{\nu}_{\mathbf{q}+\alpha\mathbf{Q}})$, accounting for the orbital symmetry of the involved exciton states. Elastic impurity scattering only causes a change in the center-of-mass momentum and no energy transfer as ensured by the δ function. Hence, the broadening of the state with the energy E^{μ} and the center-of-mass momentum $\mathbf{Q} = 0$ is caused by elastic scattering processes into the energy states $E^{\nu} + \hbar^2\mathbf{Q}^2/2M = E^{\mu}$ with the momentum transfer $\mathbf{Q}$, cf. Fig. 1. The efficiency of the scattering is given by the disorder parameter D_0 and the orbital form factor $\mathcal{F}$. Assuming that the impurity density is not sensitive to temperature $\rho_{\mathrm{d}}(T) = \rho_{\mathrm{d}}$, the impurity-induced broadening of excitonic resonances is also temperature independent.

To obtain an analytic expression for the broadening, we performed a few approximations as mentioned above. Among others, we have neglected off-resonant processes as well as impurity-induced inhomogeneous broadening. Solving Eq. (5) numerically for a significant amount of samples and averaging over the resulting spectra would reveal additional effects including an asymmetrical broadening of excitonic resonances, which is beyond the scope of this work. Here, we focus on an analytical investigation allowing us to reveal the microscopic processes behind the broadening of exciton lines.

III. RESULTS

Recent studies [26,27] demonstrated that the encapsulation of TMDs with hBN smooths out the dielectric disorder, which allows the spectral resolving of energetically close-lying excited states, revealing exciton states above $2s$. In our study we have investigated the impurity broadening of up to the $5s$ state. First, we evaluate Eq. (1) and calculate the absorption spectrum for the exemplary WS_2 monolayer, cf. Fig. 2 with an exemplary value for the disorder parameter $D_0 = 0.03$ eV. We find a clear broadening of higher excitonic states due to an efficient exciton-impurity scattering. The energetically lowest $1s$ state remains unchanged, reflecting the lack of resonant states for the elastic scattering with impurities, cf. Fig. 1. Note that this is only the case as long as one stays in the low impurity density limit, where the momentum transfer is not sufficient to scatter the excitons into possibly lower-lying dark exciton states.

To further investigate the broadening due to elastic exciton-impurity scattering, we apply the analytic expression in Eq. (9). To make our investigations independent of the disorder strength D_0, the broadenings are normalized to the linewidth of the $2s$ exciton state, cf. Fig. 3, since we are mainly interested in the qualitative behavior of the broadening with respect to the quantum index n including different scattering contributions in various TMD materials. Figure 3 illustrates different contributions governing the linewidth broadening of all bright, i.e., optically accessible, exciton states ($1s$, $2s$, $3s$, etc.). Since the impurity-induced scattering is elastic, excitons

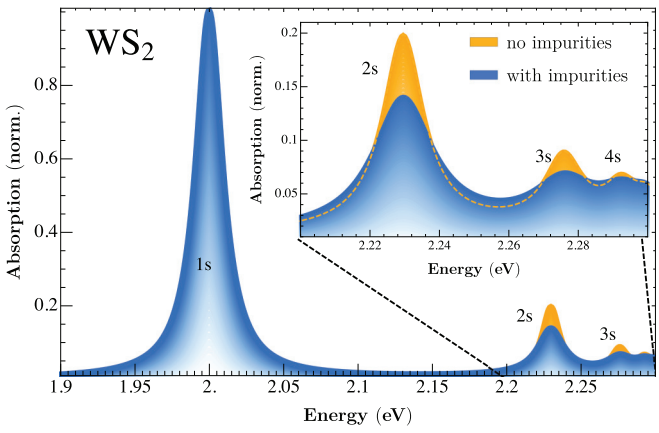

FIG. 2. Impurity-broadened absorption spectrum of WS_2 on silicon dioxide at room temperature. The inset shows a zoom-in to the higher exciton states. Broadening due to phonons and radiative losses are considered [10,25]. Adding the elastic exciton-impurity scattering, we observe no change in the $1s$ ground state, while higher excitonic states become significantly broadened. Note that the spectrum has been normalized to the intensity of the $1s$ ground state.

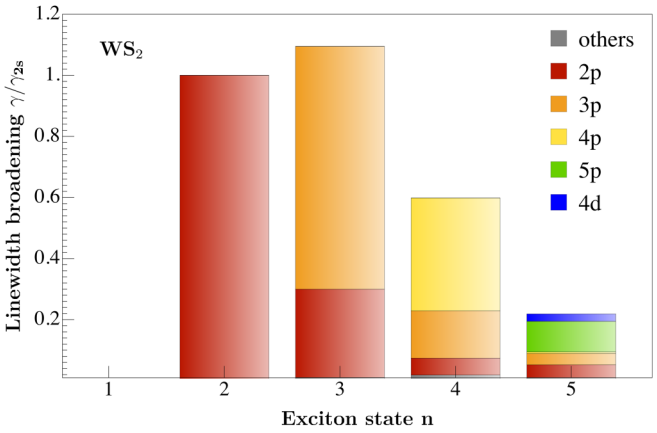

FIG. 3. Impurity-induced scattering channels contributing to the linewidth broadening of the s-type exciton states in WS_2. The values are normalized to the γ_{2s} corresponding to the width of the $2s$ exciton. This way the results are independent of the disorder strength D_0. The figure illustrates the dominant contribution of the s-p scattering. The broadening of the $3s$ state is generally higher compared to the $2s$ exciton reflecting the increased number of scattering states. However, the broadening decreases for the higher $4s$ and $5s$ states reflecting the reduced scattering efficiency.

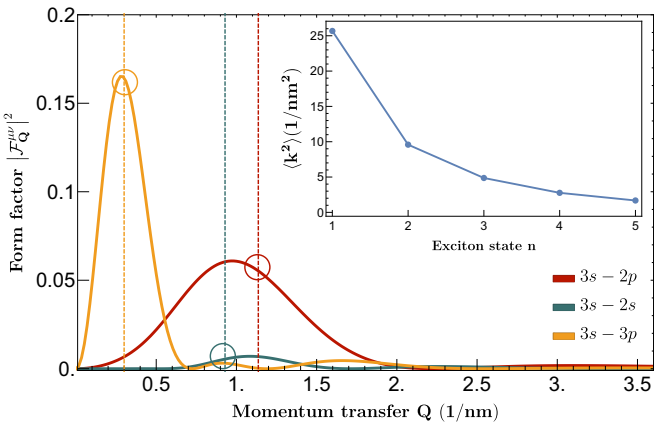

FIG. 4. Dimensionless scattering form factor $|\mathcal{F}_{\mathbf{Q}}^{\mu\nu}|^2$ for the $\mu = 3s$ exciton state as a function of the momentum transfer Q and for different in-scattering states ν. The vertical lines mark the momentum transfer Q_0 that insures the energy conservation for the elastic scattering process (Fig. 1). The inset shows the momentum uncertainty of the state as defined in Eq. (10) for the corresponding s state.

can only be scattered to lower-lying exciton parabolas, as illustrated in Fig. 1. A direct consequence is that the broadening of the $1s$ ground state is not influenced by impurity scattering, since E^{1s} is the energetically lowest state and has no resonant states to scatter into. In the case of the $2s$ state, scattering into energetically lower-lying $1s$ and $2p$ exciton parabola is possible (Fig. 1). Interestingly, the broadening of $2s$ is entirely determined by the impurity-induced transition $2s \rightarrow 2p$ (Fig. 3). Similarly, the broadening of the $3s$ ($4s$) state is also dominated by the scattering into the energetically lower p states. Only a minor contribution stems from the transition to the lower-lying s states.

To understand this behavior, we study the scattering form factor $\mathcal{F}_{\mathbf{Q}}^{\mu\nu}$ from Eq. (6), which essentially gives the scattering efficiency for the transition $\mu \rightarrow \nu$ with the required momentum transfer $\mathbf{Q}$. We illustrate the squared absolute value of the form factor for the exemplary $3s$ state, cf. Fig. 4. Here, we find three possible scattering states: the $2s$, $2p$, and $3p$ exciton parabola (Fig. 1). After discussing Fig. 3, we know that the $3s \rightarrow 3p$ transition presents the most efficient impurity-induced scattering channel. This is in line with the largest maximum in the form factor for the $3s \rightarrow 3p$ scattering process, cf. the orange line in Fig. 4. The form factor for the $3s \rightarrow 2s$ transition almost vanishes, which leads to the vanishing contribution to the linewidth, cf. the gray line in Fig. 4. The weak scattering between s states can be understood, when considering the two contributions composing the excitonic form factor. In the case of equal electron and hole masses, $\alpha \approx \beta$ the difference appearing in the excitonic form factor vanishes for isotropic wave functions (s states), but has a finite value for antisymmetric final states (e.g., p states). Note, however, that for interactions differently affecting electrons and holes, e.g., deformation potential interaction with phonons, the excitonic form factor can favor s-to-s scattering instead of s-to-p scattering. Studying Eq. (9) for the exciton linewidth broadening γ^{μ}, there is only one momentum transfer Q that fulfills the energy conservation for each scattering process $\mu \rightarrow \nu$. Therefore, the corresponding scattering matrix is evaluated only at specific values $Q_{\mu\nu}$, which are marked by a vertical dashed line in Fig. 4. From the perspective of the $3s$ state, the nearest state is the $3p$ exciton. For the required momentum transfer Q_{3s-3p}, the scattering matrix has an absolute maximum. In contrast, the value of the scattering matrix at Q_{3s-2s} is much smaller. This explains the largest linewidth contribution of the $3s$ state stemming from the scattering into the $3p$ exciton parabola (Fig. 3).

Another important observation in Fig. 3 is that the largest impurity-induced broadening is predicted for the $3s$ exciton. It is obvious that the state is broader than the $2s$ exciton due to the increased number of possible scattering partners in energetically lower-lying parabolas. However, it is not intuitive why the broadening decreases for states higher than the $3s$ exciton, in spite of the presence of more resonant states available for scattering. This can be explained by examining the momentum uncertainty of a state

$$\langle k^2 \rangle_{\mu} = \sum_{\mathbf{k}} \left|\phi_{\mathbf{k}}^{\mu}\right|^2 k^2, \tag{10}$$

which is a measure for the width of the state in momentum space and is crucial for the overlap appearing in the form factor. As the exciton radius in real space increases for higher states, the momentum uncertainty decreases (inset in Fig. 4), leading to a reduced scattering efficiency. The above discussed reduction of the scattering cross section also gives rise to a reduced exciton-phonon scattering efficiency for excited exciton states, which is in detail discussed in a previous experiment-theory study [25]. However, in contrast to the scattering with phonons, the impurity scattering requires complete energy conservation only allowing scattering to states with the same energy but different momentum. As a consequence, the scattering to a state with the same quantum index n (e.g., $2s \rightarrow 2s$), which is very efficient for phonon-mediated transitions

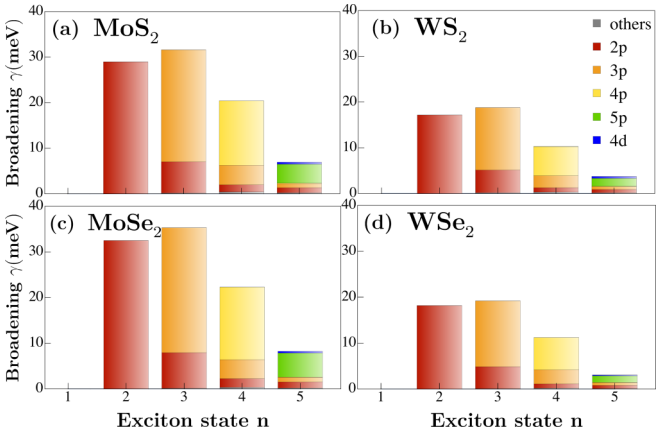

FIG. 5. Comparison of the impurity-induced exciton linewidths for different TMD materials. The broadening was calculated for an exemplary disorder parameter of $D_0 = 0.03$ eV. Generally, the contributions are similar for all investigated TMDs, since the excitonic wave functions and therefore the scattering efficiency does not vary much. The impurity-induced broadening is quantitatively smaller in tungsten-based TMDs due to their smaller effective mass.

[25] do not contribute to the impurity-induced broadening. Moreover, exciton-phonon scattering has been shown to lead to an efficient intervalley scattering [10,25]. In the case of impurity scattering, the momentum dependence results from the Fourier transform of the disorder potential. Therefore, in the case of low impurity density (correlation length $\gg$ lattice constant) the disorder potential can not provide the momentum necessary for intervalley scattering. Apart from the above mentioned differences, the derived scattering rate in Eq. (9) has the same form as the exciton-phonon scattering and the used approach can be generalized to the treatment of impurity-induced scattering of incoherent excitons with finite center of mass momentum, which, e.g., contributes to a reduction of diffusion velocity for excitons in disordered systems.

So far, we have discussed the impurity-induced homogeneous broadening of excitonic states in the exemplary WS_2 monolayer. Now, we study the comparison between the four most studied semiconducting TMDs including WS_2, WSe_2, MoS_2, and $MoSe_2$, cf. Fig. 5. Here we assume an exemplary value of $D_0 = 0.03$ eV. We find that all four TMDs behave qualitatively similar, i.e., exhibiting a maximum broadening for the $3s$ exciton and also regarding the dominant contribution stemming from scattering between s and p states. This is not surprising, since the exciton binding energies and the exciton wave functions are similar for all four TMDs. However, we observe a quantitative difference between molybdenum- and tungsten-based materials, despite the same disorder strength D_0. For tungsten-based TMDs we find clearly smaller broadening for all excitonic states. Further evaluating the momentum integral in Eq. (9) leads to $\gamma^\mu \propto \frac{M}{2\pi\hbar^2}\sum_\nu |\mathcal{F}^{\mu\nu}_{Q_{\mu\nu}}|^2$, with $Q_{\mu\nu} = \frac{1}{\hbar}\sqrt{2M(E^\mu - E^\nu)}$. Here the prefactor proportional to the total mass M reflects the density of states $(\partial E_Q/\partial Q)^{-1}$, which is higher for flat exciton dispersions. The total mass ratio between, e.g., MoS_2 and WS_2 $\frac{M_{MoS_2}}{M_{WS_2}} \approx 1.54$ is roughly the factor between the linewidth broadening of the two materials.

IV. CONCLUSION

In conclusion, we have derived an analytic expression for the spectral broadening of excitonic resonances due to elastic exciton-impurity scattering in monolayer transition metal dichalcogenides. The main findings are that (i) the scattering between s and p states is dominant reflecting an optimal overlap of excitonic wave functions, (ii) the broadening is maximal for the $3s$ state and then decreases for higher excitons due to the larger exciton radii and thus smaller scattering cross sections in momentum space, and (iii) molybdenum-based TMDs show an overall higher broadening due to their higher effective mass leading to an increased density of resonant states for impurity scattering. Our work brings new insights into possible homogeneous broadening mechanisms for higher excitonic states in TMD monolayers.

ACKNOWLEDGMENTS

We acknowledge financial support from the European Unions Horizon 2020 research and innovation program under Grant Agreement No. 785219 (Graphene Flagship) as well as from the Swedish Research Council (VR).

[1] G. Wang, A. Chernikov, M. M. Glazov, T. F. Heinz, X. Marie, T. Amand, and B. Urbaszek, *Colloquium*: Excitons in atomically thin transition metal dichalcogenides, Rev. Mod. Phys. **90**, 021001 (2018).

[2] E. Malic, M. Selig, M. Feierabend, S. Brem, D. Christiansen, F. Wendler, A. Knorr, and G. Berghäuser, Dark excitons in transition metal dichalcogenides, Phys. Rev. Mater. **2**, 014002 (2018).

[3] M. M. Ugeda, A. J. Bradley, S.-F. Shi, H. Felipe, Y. Zhang, D. Y. Qiu, W. Ruan, S.-K. Mo, Z. Hussain, Z.-X. Shen *et al.*, Giant bandgap renormalization and excitonic effects in a monolayer transition metal dichalcogenide semiconductor, Nat. Mater. **13**, 1091 (2014).

[4] K. He, N. Kumar, L. Zhao, Z. Wang, K. F. Mak, H. Zhao, and J. Shan, Tightly Bound Excitons in Monolayer WSe_2, Phys. Rev. Lett. **113**, 026803 (2014).

[5] R. Dong and I. Kuljanishvili, Review article: Progress in fabrication of transition metal dichalcogenides heterostructure systems, J. Vac. Sci. Technol. B **35**, 030803 (2017).

[6] R. Addou, S. McDonnell, D. Barrera, Z. Guo, A. Azcatl, J. Wang, H. Zhu, C. L. Hinkle, M. Quevedo-Lopez, H. N. Alshareef *et al.*, Impurities and electronic property variations of natural MoS_2 crystal surfaces, ACS nano **9**, 9124 (2015).

[7] G. Moody, C. K. Dass, K. Hao, C.-H. Chen, L.-J. Li, A. Singh, K. Tran, G. Clark, X. Xu, G. Berghäuser *et al.*, Intrinsic homogeneous linewidth and broadening mechanisms of excitons in

monolayer transition metal dichalcogenides, Nat. Commun. **6**, 8315 (2015).

[8] C. Pöllmann, P. Steinleitner, U. Leierseder, P. Nagler, G. Plechinger, M. Porer, R. Bratschitsch, C. Schüller, T. Korn, and R. Huber, Resonant internal quantum transitions and femtosecond radiative decay of excitons in monolayer WSe_2, Nat. Mater. **14**, 889 (2015).

[9] P. Dey, J. Paul, Z. Wang, C. E. Stevens, C. Liu, A. H. Romero, J. Shan, D. J. Hilton, and D. Karaiskaj, Optical Coherence in Atomic-Monolayer Transition-Metal Dichalcogenides Limited by Electron-Phonon Interactions, Phys. Rev. Lett. **116**, 127402 (2016).

[10] M. Selig, G. Berghäuser, A. Raja, P. Nagler, C. Schüller, T. F. Heinz, T. Korn, A. Chernikov, E. Malic, and A. Knorr, Excitonic linewidth and coherence lifetime in monolayer transition metal dichalcogenides, Nat. Commun. **7**, 13279 (2016).

[11] A. Chernikov, T. C. Berkelbach, H. M. Hill, A. Rigosi, Y. Li, O. B. Aslan, D. R. Reichman, M. S. Hybertsen, and T. F. Heinz, Exciton Binding Energy and Nonhydrogenic Rydberg Series in Monolayer WS_2, Phys. Rev. Lett. **113**, 076802 (2014).

[12] H. Haug and S. W. Koch, *Quantum Theory of the Optical and Electronic Properties of Semiconductors*, 5th ed. (World Scientific, Singapore, 2004).

[13] M. Hirtschulz, F. Milde, E. Malić, S. Butscher, C. Thomsen, S. Reich, and A. Knorr, Carbon nanotube Bloch equations: A many-body approach to nonlinear and ultrafast optical properties, Phys. Rev. B **77**, 035403 (2008).

[14] E. Malic, J. Maultzsch, S. Reich, and A. Knorr, Excitonic Rayleigh scattering spectra of metallic single-walled carbon nanotubes, Phys. Rev. B **82**, 115439 (2010).

[15] E. Malic and A. Knorr, *Graphene and Carbon Nanotubes: Ultrafast Optics and Relaxation Dynamics* (John Wiley & Sons, New York, 2013).

[16] M. Kira and S. W. Koch, Many-body correlations and excitonic effects in semiconductor spectroscopy, Prog. Quantum Electron. **30**, 155 (2006).

[17] F. Rossi and T. Kuhn, Theory of ultrafast phenomena in photoexcited semiconductors, Rev. Mod. Phys. **74**, 895 (2002).

[18] E. Malic, G. Berghäuser, M. Feierabend, and A. Knorr, Optical response from functionalized atomically thin nanomaterials, Ann. Phys. (NY) **529**, 1700097 (2017).

[19] E. Runge and R. Zimmermann, Optical properties of localized excitons in nanostructures: Theoretical aspects, in *Advances in Solid State Physics 38*, edited by B. Kramer (Springer, Berlin, 1999), pp. 251–263.

[20] S. Glutsch and F. Bechstedt, Theory of asymmetric broadening and shift of excitons in quantum structures with rough interfaces, Phys. Rev. B **50**, 7733 (1994).

[21] A. Thränhardt, S. Kuckenburg, A. Knorr, T. Meier, and S. W. Koch, Quantum theory of phonon-assisted exciton formation and luminescence in semiconductor quantum wells, Phys. Rev. B **62**, 2706 (2000).

[22] G. Berghäuser and E. Malic, Analytical approach to excitonic properties of MoS_2, Phys. Rev. B **89**, 125309 (2014).

[23] V. M. Axt and T. Kuhn, Femtosecond spectroscopy in semiconductors: A key to coherences, correlations and quantum kinetics, Rep. Prog. Phys. **67**, 433 (2004).

[24] F. Wendler, A. Knorr, and E. Malic, Carrier multiplication in graphene under Landau quantization, Nat. Commun. **5**, 3703 (2014).

[25] S. Brem, J. Zipfel, M. Selig, A. Raja, L. Waldecker, J. Ziegler, T. Taniguchi, K. Watanabe, A. Chernikov, and E. Malic, Intrinsic lifetime of higher excitonic states in Tungsten diselenide monolayers, Nanoscale **11**, 12381 (2019).

[26] F. Cadiz, E. Courtade, C. Robert, G. Wang, Y. Shen, H. Cai, T. Taniguchi, K. Watanabe, H. Carrere, D. Lagarde *et al.*, Excitonic Linewidth Approaching the Homogeneous Limit in MoS_2-Based van der Waals Heterostructures, Phys. Rev. X **7**, 021026 (2017).

[27] O. A. Ajayi, J. V. Ardelean, G. D. Shepard, J. Wang, A. Antony, T. Taniguchi, K. Watanabe, T. F. Heinz, S. Strauf, X. Y. Zhu *et al.*, Approaching the intrinsic photoluminescence linewidth in transition metal dichalcogenide monolayers, 2D Mater. **4**, 031011 (2017).